



A structural and optical properties of Cu-doped ZnO films prepared by spray pyrolysis

Sabrina Roguai^{1,2} · Abdelkader Djelloul^{1,2}

Received: 22 October 2019 / Accepted: 9 January 2020 / Published online: 23 January 2020
© Springer-Verlag GmbH Germany, part of Springer Nature 2020

Abstract

Pure and Cu doped ZnO films were grown by ultrasonic spray pyrolysis onto glass substrates at 450 °C for 30 min. This study aims to investigate the influence of Cu doping content [0.02–0.20] on structural, microstructural and optical properties. X-ray diffraction analysis reveals a structural disorder depending on Cu loading besides the appearance of CuO phase. The doping effectiveness is revealed by EDX analysis of the chemical composition of the films. The transmittance shows a decreasing tendency with increasing Cu concentration. The refractive indices increase, whereas the values of forbidden energy gap decrease with the increase in Cu dopant concentration.

Keywords Thin films · X-ray diffraction · Optical properties

1 Introduction

Zinc oxide semiconductor films have been very useful, particularly in the field of spintronics, because of their wide band gap ($E_g = 3.31$ eV), exciton band energy (60 meV) at room temperature [1] besides its significant transmittance value of 0.9 in the visible region. ZnO crystallizes within a wurtzite-type structure defined by a hexagonal lattice where Zn^{2+} ions occupy the tetrahedral sites formed by O^{2-} ions. Numerous researches have already fabricated ZnO films using various techniques, including spray pyrolysis [2], reactive magnetron sputtering [3, 4], chemical vapor deposition (CVD) [5], sol–gel [6] molecular beam epitaxy [7], and pulsed laser deposition [8, 9].

Recently, the doping of semiconductors by transition metals is of great importance, because of their unusual optical properties and promising potential for optoelectronic applications [10–13]. The doping of ZnO with metal ions has been found to influence its structure and particularly its

physical properties such as particle size, dislocation density, bond length, strain deformation, etc. [14, 15].

Copper (Cu) element is of particular interest, thanks to its low toxicity and large abundance [9, 16]. The incorporation of Cu within ZnO host lattice has been found to enhance its physical and chemical properties, such as photocatalysis activity, gas sensitivity, magnetic susceptibility, optical and electrical properties [14, 17].

In this work, thin films of pure and Cu doped ZnO films are deposited by ultrasonic spray pyrolysis (USP) technique onto glass substrates ($30 \times 12 \times 1.2$ mm³) at 450 °C for 30 min. The effects of the doping on structure, microstructure and optical properties are discussed.

2 Experimental part

2.1 Film preparation

In this study, the use of ultrasonic pyrolytic spray technique for the deposition of thin films of ZnO, $Zn_{1-x}Cu_xO$ [$x = 2, 5, 10, 15$ and 20 at%], offers various benefits, such as better homogeneity, low-power processing, easy-to-control stoichiometry, and large surface covering. Zinc acetate [$Zn(CH_3COO)_2 \cdot 2H_2O$] (Fulka 99.9%) (0.01 M) and copper chloride ($CuCl_2 \cdot 2H_2O$) (2–20) (Cu, at%) as precursors are dissolved in 20 ml methanol (Merck 99.5%), 30 ml ethanol (Merck 99.5%). This mixture has been chosen for its easy

✉ Sabrina Roguai
rog.sabrina@yahoo.fr

¹ LASPI2A Laboratoire Des Structures, Propriétés Et Interactions Inter Atomiques, Université Abbes Laghrour, Khenchela 40000, Algérie

² Science of Matter, Abbes Laghrour University, Khenchela, Algeria

processing, fluidity, fast transformation, and precursor fog in steam. 50 ml deionized water (resistivity = 18.2 MΩ cm) has been added as oxidizing agent. A small amount of acetic acid is added to the aqueous solution for adjusting the pH to about 4.8 to prevent the formation of hydroxides. This solution containing various constituents is then deposited after being sprayed in fine drops, by an atomizer using a 40 kHz ultrasonic generator with the power of 130 W. This system makes it possible to transform the solution into a jet of very small droplets, i.e. fine drop of 45 μm for a frequency of 40 kHz. The remaining experimental conditions are kept fixed: the distance separating the substrate from the end of the pipe 5 cm, the solution stream rate 0.1 ml/min, surface of glass substrate (30 × 12 × 1.2 mm³), deposition temperature 450 °C, and deposition time 30 min. The temperature of the substrate has been monitored by a thermocouple and electronically registered [18].

2.2 Characterization techniques

The structure of the films is characterized by X-ray diffraction (Rigaku Ultima IV equipped with Cu–Kα radiation, 0.15418 nm). The morphology of the films was checked by scanning electron microscopy (Quanta™ 250 FEG-SEM from FEI company) equipped with energy dispersive X-ray spectroscopy (EDS) for chemical analysis. The optical properties are determined by measuring the transmittance of the films using a SpectroScan 80D spectrophotometer UV–vis in the 190–1100 nm spectral range.

3 Results and discussion

3.1 Structure and microstructure analysis

The XRD spectra of pure and copper-doped ZnO (2, 5, 10, 15 and 20 at%) are illustrated in Fig. 1, which shows that the films obtained are zinc oxide (ZnO). We find almost all the typical diffraction peaks of powdered ZnO which crystallizes in the wurtzite structure with a preferential grains orientation to the *c* axis which is perpendicular to the surface of the substrate. This information was obtained using reference code (01-097-0207) and was easily indexed in hexagonal wurtzite phase with *P63mc* space group and JCPDS card (36-1451) [19]. These diffraction peaks corresponding to (100), (002), (101), (102), (110), (103) and (112) planes of ZnO lattice are present in all spectra. No secondary phase corresponding to copper oxide (CuO) is observed within doped films ($x_{\text{Cu}} \leq 0.10$). For the 15 and 20 at% doped films we noticed that a new peak emerges respectively at 38.47° and 38.60° corresponds to (111) that belongs to the CuO phase (JCPDS#05-0661) [20, 21], which are in agreement with the literature showing the presence of a wurtzite type

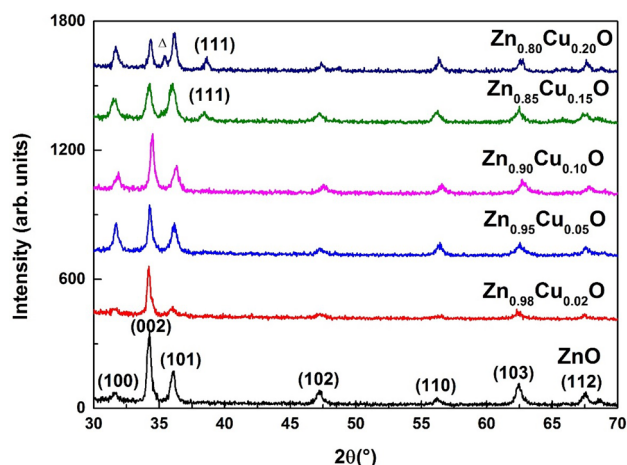


Fig. 1 XRD patterns of ZnO and Zn_{1-x}Cu_xO (with $x=2, 5, 10, 15$ and 20 at%) films

phase for a copper doping rate lower by 15 at%, while those with a higher copper content include a tenorite type oxide phase (Zn_xCu_{1-x}O) [22]. Which means the Cu-doping concentration limit in ZnO is around $x_{\text{Cu}} = 0.15$ in our experiment settings.

Compared to the undoped ZnO, the intensity and the positions of the diffraction peaks vary considerably and non-homogeneously following the increase in the doping level illustrated by the decrease in the intensity of the peaks in the doped ZnO, and we note as well that the peak (002) has been shifted to a higher value of 34.26°–34.29°. This shift shows the substitution of Zn by Cu in the hexagonal lattice prompting the decrease in the crystallinity of ZnO [23–25]. On the other hand, the intensity of the peak (101) increases proportionally with the doping confirming the substitution of Zn²⁺ by Cu²⁺ with the preservation of the preferred orientation in the hexagonal structure of copper-doped ZnO films perhaps because of the ionic radius difference [26–29]. Moreover, at the doping rate (20 at.%), the presence of impurity in the turn of 35.39° was noticed, which explains, firstly, that the Cu would not be more interstitial but more likely to be fused in clusters of metallic copper and, secondly, interprets the dissuasive effect on the peak (002), but it remains energetically a favorable factor [30–32]. Which confers that the interstitial substitution of Cu²⁺ influence on the concentration of interstitial Zn, oxygen and Zn vacancies [27, 33]. It is suggested that the incorporation of Cu²⁺ into the ZnO structure is done regularly if enters octahedral interstitial sites since tetrahedral coordination is not favorable for this species [22, 34].

For a doping rate < 15 at% we observe the presence of a single-phase Zn_{1-x}Cu_xO material having the wurtzite (hexagonal) structure of ZnO with a linear variation of the lattice parameters “*a*” and “*c*”, then decreases for 15 at% and

20 at% with the presence of additional peaks corresponding to Cu, CuO or any other impurity in X-ray diffraction patterns at $2\theta=38.47^\circ$ and 38.60° for 15 at% and 20 at%, respectively. This indicates that the Cu atoms were scattered in the ZnO and substituted Zn, thus increasing the lattice parameter (Table 1) [35]. This modification of lattice parameters confirming that the substitution in the tetrahedron coordinate is caused by the ionic radius of Cu^{2+} (ionic radius = 0.057 nm) which is smaller than the Zn^{2+} sites (ionic radius = 0.060 nm) [27, 36].

The real distance between two Zn atoms in the studied systems is about 0.326 nm, while the Zn atoms in ZnO are present in tetrahedral structures with Zn–O distances of 0.196 nm. For uniformly distributed Cu ions, the mean distance between Cu ions that have been substituted into Zn sites within ZnO crystal lattice can be estimated via [37] $N_{\text{at}} = (4/3) (Z/V_C) \pi r^3$, where r is the average radius of an atomic sphere and N_{at} is the number of atoms in the sphere. Figure 2 shows the number of zinc atoms in a sphere with a radius of r . The structural parameters for $\text{Zn}_{0.98}\text{Cu}_{0.02}\text{O}$ are: $a = 0.3254$ nm, $c = 0.5212$ nm; volume of unit cell (V_C) = 47.79×10^{-3} nm³; $Z = 2$. For zinc atoms in a wurtzite structure of $\text{Zn}_{0.98}\text{Cu}_{0.02}\text{O}$, $Z/V_C = 41.84$ nm⁻³. In $\text{Zn}_{0.98}\text{Cu}_{0.02}\text{O}$ film, 2% of zinc sites are occupied by Cu ions. Therefore, the 50th zinc site from the probe atom is occupied by Cu. Using the above calculation, the average distance between Cu ions is estimated to be around 0.65 nm, which means that the nearest Cu ion to a probe Cu ion is located in the next unit cell. On the other hand, In the $\text{Zn}_{0.80}\text{Cu}_{0.20}\text{O}$ film, the fifth zinc site from the probe atom is occupied by Cu, the mean distance of Cu–Cu pairs is 0.30 nm. This is consistent with the XRD results.

The estimation of the micro-stress (ϵ) using the (Eq. (1)) [38]:

$$\epsilon = \frac{\beta \cos(\theta)}{4} \tag{1}$$

where β is the angular peak width at half maximum in radian along (002) plane, and θ is Bragg’s diffraction angle.

The micro-stress of the Cu-doped sample increases at $x_{\text{Cu}} = 15$ at%, then reaches the minimum when $x_{\text{Cu}} = 0.20$ at%, the atoms trapped in the non-equilibrium position could shift to a greater positional equilibrium [27].

The parameters of the microstructure are calculated using the Scherrer formula to estimate the average crystallite size (D) (Eq. (2)) [39]:

$$D = \frac{0.9 \lambda}{\beta \cos(\theta)} \tag{2}$$

where λ is the wavelength of the incident X-ray (Cu K α radiation, $\lambda = 1.5418$ Å), β is the total half-height width (FWHM) of the peak XRD and θ is the maximum of the Bragg diffraction peak (in radians). The calculation (the results are reported in Table 2) shows that the crystallite size values are increasing for a doping level (2, 5 and 10 at%) then it goes down at (15 and 20 at%). This decrease can be interpreted by the segregation of Cu atoms in the grain boundaries due to the increase in surface energy density. The

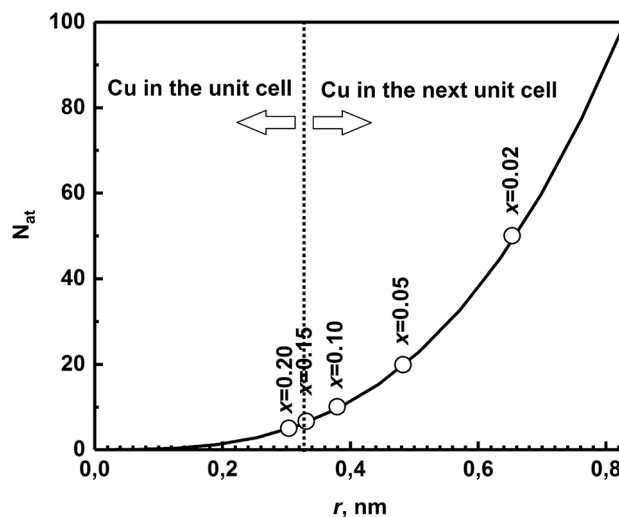


Fig. 2 The number of zinc atoms in a sphere with a radius of r for wurtzite ZnO

Table 1 X-ray diffraction data (2θ , FWHM, d-spacing, cell parameters ‘ a ’ and ‘ c ’, c/a ratio, average crystallite size (D) and micro-strain (ϵ) of different $\text{Zn}_{1-x}\text{Cu}_x\text{O}$ thin films)

$\text{Zn}_{1-x}\text{Cu}_x\text{O}$ “Nominal” Cu content (at)	2θ ($^\circ$) value (002)	FWHM (β) ($^\circ$)	D value (Å)	$a = b$ (Å)	c (Å)	c/a ratio	Average crystallite size (D) (nm)	Micro-strain (%)
$x = 0$	34.234	0.343	2.614	3.256	5.229	1.605	24.3	0.14
$x = 0.02$	34.207	0.247	2.606	3.254	5.212	1.601	33.8	0.10
$x = 0.05$	34.301	0.296	2.614	3.245	5.229	1.611	28.2	0.12
$x = 0.10$	34.470	0.321	2.601	3.239	5.202	1.606	26.1	0.13
$x = 0.15$	34.236	0.442	2.614	3.274	5.229	1.597	18.9	0.18
$x = 0.20$	34.350	0.313	2.614	3.275	5.229	1.596	26.6	0.13

Table 2 Composition and stoichiometry of the thin films obtained by statistical analysis of EDS spectra

Zn _{1-x} Cu _x O “Nominal” Cu content (at)	Zn (at.%)	Cu (at.%)	O (at.%)	<i>x</i> (Cu) “EDS” Cu content (at)
<i>x</i> =0.02	61.6	1.5	36.9	0.0237
<i>x</i> =0.05	53.8	3	43.2	0.0528
<i>x</i> =0.10	49.6	5.9	44.5	0.1063
<i>x</i> =0.15	36.7	6.5	56.8	0.1504
<i>x</i> =0.20	34.5	9	56.5	0.2068

crystallite sizes were in the 18–40 nm range; these results are in agreement with those found in the literature [22, 27, 40].

SEM images sample pure and copper-doped ZnO (2–20 at%) are shown in Fig. 3. For pure ZnO and Zn_{1-x}Cu_xO films (*x* < 15 at%) having a homogeneous surface morphology

with the particles containing the mixer of spheroid-like and rod-like particles with diameters ranging from 20 to 100 nm, confirmed the dominance of the wurtzite phase. For a Cu doping rate (15 at% and 20 at%) reveal a net change of the surface with cylindrical shape and size [22], varying between 90 and 100 nm, with an average particle size of 43 nm due to the presence of defects and deformed crystal-line structures due to the substitution of Cu [27].

The results obtained from the energy-dispersive X-ray spectroscopy are given in Fig. 4. The EDX spectra of copper-doped ZnO show the coexistence of Zn, Cu, O with the presence of foreign elements in Si, Ca, Mg synthesized deposits appearing as minor peaks belonging to the soda-lime glass substrate. The latter varies from one sample to another because of the variation in the thickness of the Cu-doped ZnO films [41]. The height of the Cu peak increases with the doping rate, which shows that Cu has been successfully doped with ZnO [18, 27].

Fig. 3 High-resolution SEM images of **a** pure ZnO film and **b–f** Cu-doped Zn_{1-x}Cu_xO thin films. The images **b–f** correspond to the Cu atomic content of 2%, 5%, 10%, 15% and 20%, respectively

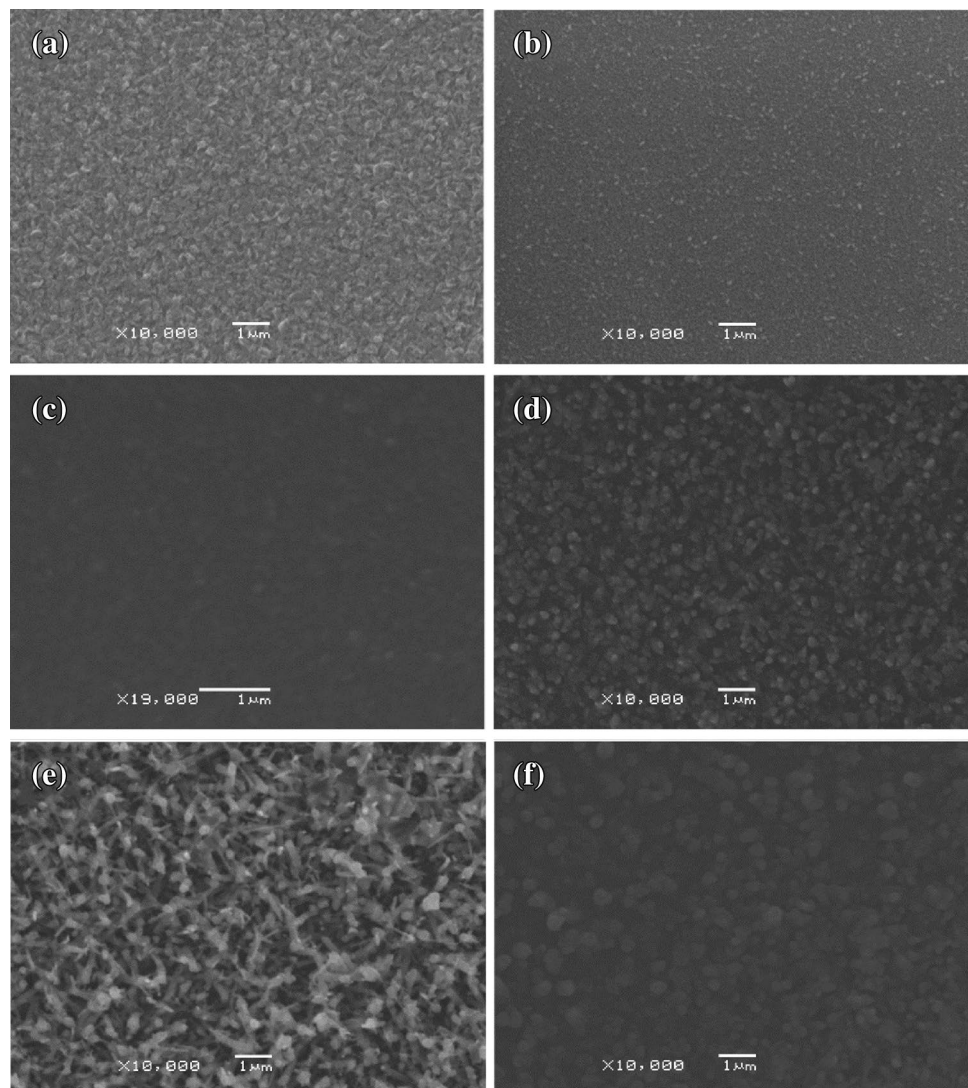
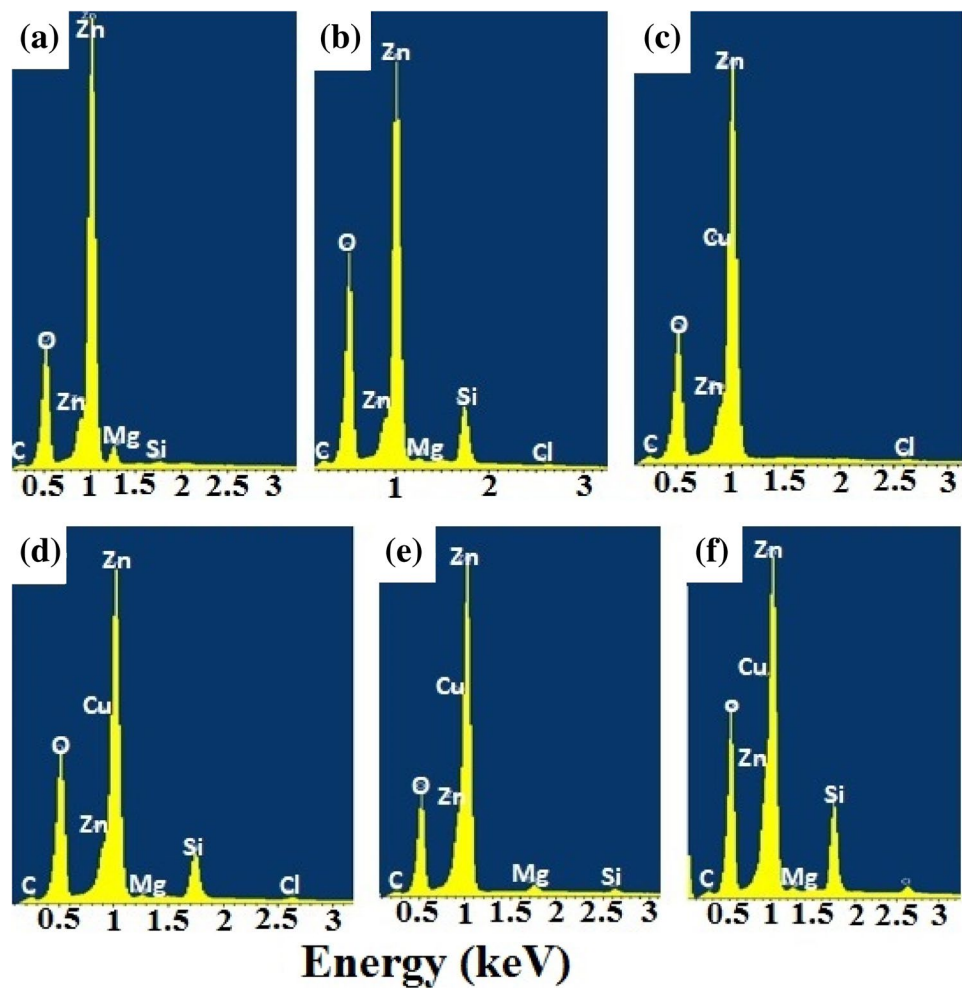


Fig. 4 EDX elemental composition analysis of **a** pure ZnO film and **b–f** Cu-doped Zn_{1-x}Cu_xO thin films. The images **b–f** correspond to the Cu atomic content of 2%, 5%, 10%, 15% and 20%, respectively



Suppose stoichiometric films of the form Zn_{1-x}Cu_xO. The stoichiometric of the films is measured exclusively from the Cu and Zn signals. According to the following relation (Eq. (3)):

$$x = r / (1 + r), \tag{3}$$

where x represents the Cu atom content and r the ratio of the Zn and Cu EDS signals (see Table 2). The incorporation of the copper in the high network is very clear, for all the doping levels, in Fig. 5, which presents the ratio of the EDS signals of Cu as a function of the calculation of the atomic content of Cu, which shows the doping efficiency with the copper.

3.2 Optical properties

Figure 6 shows the transmittance spectra for Cu doped ZnO thin films with different Cu concentration. The spectra of Zn_{1-x}Cu_xO films are taken at room temperature to study their optical properties. The dispersion parameters of the films were evaluated using a single-effective-oscillator

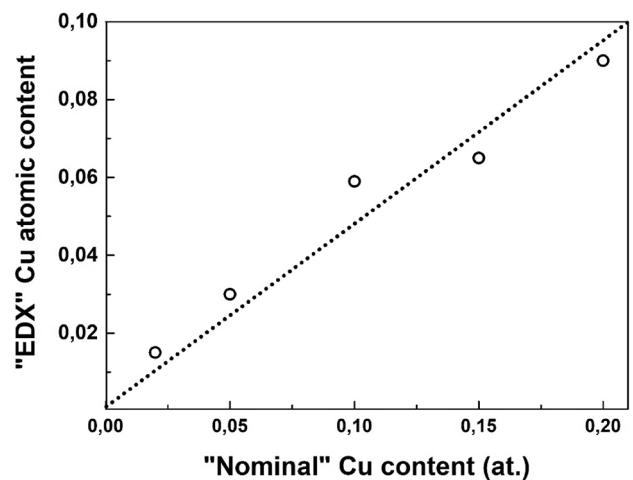


Fig. 5 The calculated Cu atomic content (from EDS analysis) plotted as function of the expected Cu content/doping

fit, proposed by Wemple and DiDomenico [18, 42]. The solid curves in Fig. 6 correspond to the curve fitting and the symbols represent the experimental data. The figure

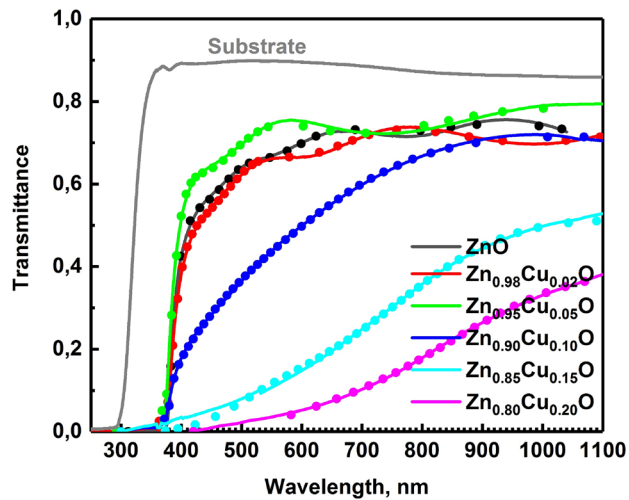


Fig. 6 Transmission spectra of ZnO and $Zn_{1-x}Cu_xO$ (with $x=2, 5, 10, 15$ and 20 at%) and transmittance of the bare glass substrate. Measured (full circles) and calculated (solid lines) transmittance spectra of films

Table 3 Dispersion parameters of the films extracted by fitting the experimental data [18]

	Thickness (nm)	E_g (eV)	n at 598 nm	n_∞
ZnO	573	3.243	1.71	1.63
$Zn_{0.98}Cu_{0.02}O$	422	3.223	1.82	1.75
$Zn_{0.95}Cu_{0.05}O$	300	3.248	1.81	1.74
$Zn_{0.90}Cu_{0.10}O$	208	3.254	1.92	1.84
$Zn_{0.85}Cu_{0.15}O$	179	2.430	2.64	2.62
$Zn_{0.80}Cu_{0.20}O$	178	1.907	2.95	2.44

reveal a reasonably good fitting to the experimental data, the values of d , E_g , n at 598 nm, and n_∞ extracted by fitting [18] the experimental data are listed in Table 3. The transmittance shows a decreasing tendency with increasing Cu concentration. The average value of transmittance decreases from 75 to 5% as the dopant concentration increases from 5–20%. This can be attributed to the incorporation of Cu^{2+} ions, which replaces the substitutional or interstitial Zn^{2+} ions from the host lattice. The dopant ion (Cu^{2+}) transforms the colourless host lattice (ZnO) into brown. In the visible region when the defects increase the absorption takes maximum values and the transmittance decreases [43].

Figure 7 presents the calculated refractive indices [18] of $Zn_{1-x}Cu_xO$ films. It is worthy to note that the refractive indices of the films increases with increase in Cu dopant concentration. The refractive index is sensitive to structural defects (e.g. voids, dopants, inclusions) [18]. Therefore, this change may be due to the effect of Cu incorporation [44] which increases the impurities in the host material.

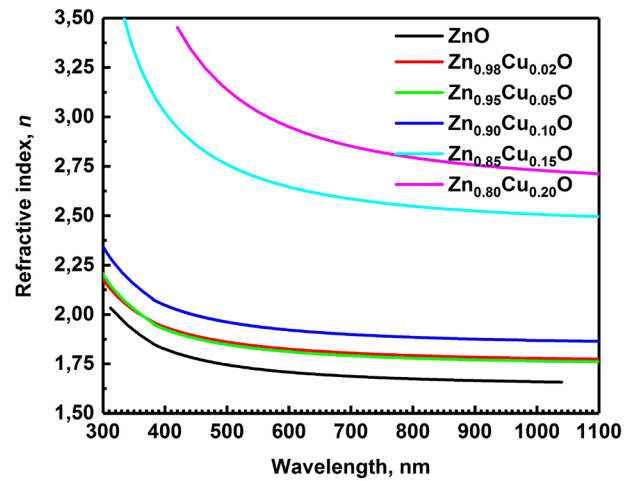


Fig. 7 Refractive index of ZnO and $Zn_{1-x}Cu_xO$ (with $x=2, 5, 10, 15$ and 20 at%) films

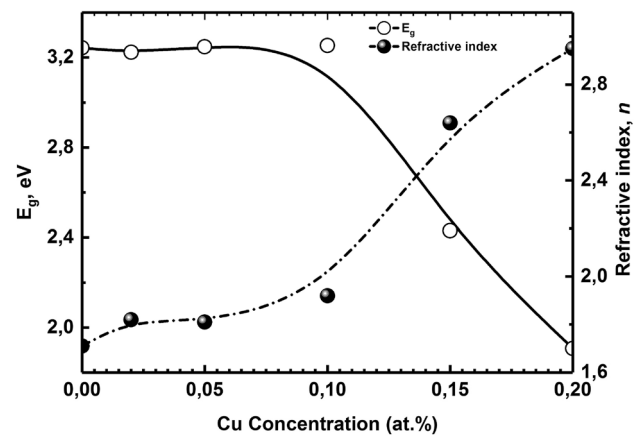


Fig. 8 Energy band gap and refractive index as function of the Cu concentration

Figure 8 shows the energy band gap and refractive index as function of the Cu concentration. It is interesting to note that the band gap of the films decreases with increase in Cu dopant concentration. The Cu $3d$ orbital is much shallower than the Zn $3d$ orbital. When a Cu atom occupies a Zn site in ZnO, it introduces two main effects: (1) the strong $d-p$ coupling between Cu and O moves O $2p$ up, which narrows the direct fundamental band gap and (2) the Cu $3d$ orbital creates impurity bands above the ZnO valence band. As a result, this exchange interaction gives rise to a negative and a positive correction to the energy of the conduction band and valence band respectively. These facts may be related to the red shift of E_g values by Cu-doping in ZnO thin films. The transitions from the impurity bands to conduction bands are usually a mixture of direct and indirect. Thus, for heavily doped ZnO:Cu thin films, their optical band gap contains

two parts—the direct fundamental band gap and the mixed impurity band gap [45]. The measured optical band gap for pure ZnO films was 3.24 eV, which is consistent with the results reported elsewhere [46]. The direct optical band gaps measured for $\text{Zn}_{1-x}\text{Cu}_x\text{O}$ films gradually decreased from 3.25 to 1.90 eV with the increase of the Cu concentration, as shown in Fig. 8. These results are in agreement with the theoretical calculations based on the functional density theory (DFT) which shows the reduction of the Cu-doped ZnO optical band gap [47]. Finally, the refractive index of $\text{Zn}_{1-x}\text{Cu}_x\text{O}$ thin films increases with decreasing energy band gap.

4 Conclusion

Cu-doped ZnO thin films were deposited on glass substrates by ultrasonic spray pyrolysis. The XRD spectra of $\text{Zn}_{1-x}\text{Cu}_x\text{O}$ indicate that the films are polycrystalline in nature. The Cu doping into ZnO solid solution is found to influence considerably the film morphology, the grain size, and the stoichiometry of the oxide. The doping effectiveness is revealed by EDX analysis of the chemical composition of the films and it shows good agreement between the expected and measured Cu atomic content. The transmittance shows a decreasing tendency with increasing Cu concentration. The refractive indices increase, whereas the values of forbidden energy gap decrease with the increase in Cu dopant concentration.

Acknowledgements The authors would like to thank the National Project Research (PNR) and LASPI²A Laboratory of Khenchela University (Algeria) for their financial support of this research project.

References

1. S. Oktik, Low cost, non-vacuum technique for the preparation of thin/thick films for photovoltaic. *Prog. Cryst. Growth. Char.* **17**, 171–240 (1988)
2. Y. Caglar, S. Aksoy, S. Ilican, M. Caglar, Crystalline structure and morphological properties of undoped and Sn doped ZnO thin films. *Superlattices. Microstruct.* **46**, 469–475 (2009)
3. L.P. Peng, L. Fang, X.F. Yang, Y.J. Li, Q.L. Huang, F. Wu, C.Y. Kong, Effect of annealing temperature on the structure and optical properties of In-doped ZnO thin films. *J. Alloys. Comp.* **484**, 575–579 (2009)
4. X.C. Wang, X.M. Chen, B.H. Yang, Microstructure and optical properties of polycrystalline ZnO films sputtered under different oxygen flow rates. *J. Alloys. Comp.* **488**, 232–237 (2009)
5. G. Zhu, G. Shulin, S. Zhu, S. Huang, G. Ran, J. Ye, Y. Zheng, Optimization study of metal-organic chemical vapor deposition of ZnO on sapphire substrate. *J. Cryst. Growth.* **349**, 6–11 (2012)
6. S. Aksay, Y. Caglar, S. Ilican, M. Caglar, Sol-gel derived zinc oxide films: effect of deposition parameters on structure, microstructure and photoluminescence properties. *Superlattices Microstruct.* **50**, 470–479 (2011)
7. S.J. Jiao, Y.M. Lu, D.Z. Shen, Z.Z. Zhang, B.H. Li, ZhH Zheng, B. Yao, J.Y. Zhang, D. Zhao, X.W. Fan, Donor-acceptor pair luminescence of nitrogen doping p-type ZnO by plasma-assisted molecular beam epitaxy. *J. Lumines.* **122**(123), 368–370 (2007)
8. A.I. Savchuk, V.I. Fediv, S.A. Savchuk, A. Perrone, Growth and characterization of ZnMnO thin films. *Superlattices Microstruct.* **38**, 421–427 (2005)
9. ChY Tsay, KSh Fan, ChM Lei, Synthesis and characterization of sol-gel derived gallium-doped zinc oxide thin films. *J. Alloys. Comput.* **512**, 216–222 (2012)
10. H.M. Yang, S. Nie, Preparation and characterization of Co-doped ZnO nanomaterials. *J. Mater. Chem. Phys.* **114**, 279–282 (2009)
11. M. Yang, Z.X. Guo, K.H. Qiu, J.P. Long, G.F. Yin, D.G. Guan, S.T. Liu, S.J. Zhou, Synthesis and characterization of Mn-doped ZnO column arrays. *Appl. Surf. Sci.* **256**, 4201–4205 (2010)
12. H. Saal, T. Bredow, M. Binnewies, Band gap engineering of ZnO via doping with manganese: effect of Mn clustering. *J. Phys. Chem. Chem. Phys.* **11**, 3201–3209 (2009)
13. G.M. Kumar, P. Ilanchezhian, J. Kawakita, M. Subramanian, R. Jayavel, Magnetic and optical property studies on controlled low-temperature fabricated one dimensional Cr doped ZnO nanorods. *J. Cryst. Eng. Commun.* **12**, 1887–1892 (2010)
14. S. Singhal, J. Kaur, T. Namgyal, R. Sharma, Cu-doped ZnO nanoparticles: synthesis, structural and electrical properties. *Phys. B* **407**, 1223–1226 (2012)
15. T. Das, K.B. Das, K. Parashar, R. Kumar, H.K. Choudhary, A.V. Anupama, B. Sahoo, P.K. Sahoo, S.K.S. Parashar, Effect of Sr-doping on sintering ability, morphology, structure, photocatalytic activity and AC conductivity of ZnO ceramics. *J. Mater. Sci. Mater. Electron.* **28**, 13587–13595 (2017)
16. B.E. Filali, T.V. Torchynsk, A.I.D. Cano, Photoluminescence and Raman scattering study in ZnO: Cu nanocrystals. *J. Lumin.* **161**, 25–30 (2015)
17. N.E. Sung, S.W. Kang, H.J. Shin, H.K. Lee, I.J. Lee, Cu doping effects on the electronic and optical properties of Cu-doped ZnO thin films fabricated by radio frequency sputtering. *Thin Solid Films* **547**, 285–288 (2013)
18. S. Roguai, A. Djelloul, C. Nouveau, T. Souier, A. A. Dakhel, M. Bououdina, Structure, microstructure and determination of optical constants from transmittance data of co-doped $\text{Zn}_{0.90}\text{Co}_{0.05}\text{Mn}_{0.05}\text{O}$ (M = Al, Cu, Cd, Na) films. *J. Alloys Compd.* **599**, 150–158 (2014).
19. J.S. Ghomi, M.A. Ghasemzadeh, S. Zahedi, ZnO nanoparticles a highly effective and readily recyclable catalyst for the one pot synthesis of 1,8-dioxo-decahydroacridine and 1,8-dioxoctahydro-xanthene derivatives. *J. Mex. Chem. Soc.* **57**, 1–7 (2013)
20. J. Langford, D. Louer, High-resolution powder diffraction studies of copper (II) oxide. *J. Appl. Crystallogr.* **24**, 149–155 (1991)
21. P.K. Sharma, M. Kumar, A.C. Pandey, Green luminescent ZnO:Cu²⁺ nanoparticles for their applications in white-light generation from UV LEDs. *J. Nanoparticle Res.* **13**, 1629–1637 (2011)
22. D.M. Fernandes, R. Silva, A.A.W. Hechenleitner, E. Radovanovic, M.A.C. Melo, E.A.G. Pineda, Synthesis and characterization of ZnO, CuO and a mixed Zn and Cu oxide. *Mater. Chem. Phys.* **115**, 110–115 (2009)
23. T.S. Herng, S.P. Lau, S.F. Yu, H.Y. Yang, L. Wang, M. Tanemura, J.S. Chen, Magnetic anisotropy in the ferromagnetic Cu-doped ZnO nanoneedles. *J. Appl. Phys.* **90**, 032509 (2007)
24. Z. Zhang, J.B. Yi, J. Ding, L.M. Wong, H.L. Seng, S.J. Wang, J.G. Tao, G.P. Li, G.Z. Xing, T.C. Sum, C.H.A. Huan, T. Wu, Cu-doped ZnO nanoneedles and nanonails: morphological evolution and physical properties. *J. Phys. Chem. C.* **112**, 9579–9585 (2008)
25. O. Lupan, Th Pauporté, T. Le Bahers, B. Viana, I. Ciofini, Wavelength emission tuning of ZnO nanowires-based light emitting diodes by Cu-doping: experimental and computational insights. *Adv. Funct. Mater.* **21**, 3564–3572 (2011)

26. L. Ma, S. Ma, H. Chen, X. Ai, X. Huang, AMicrostructures and optical properties of Cu-doped ZnO films prepared by radio frequency reactive magnetron sputtering. *Appl. Surf. Sci.* **257**, 10036–10041 (2011)
27. S. Muthukumar, R. Gopalakrishnan, Structural, FTIR and photoluminescence studies of Cu doped ZnO nanopowders by coprecipitation method. *Opt. Mater.* **34**, 1946–1953 (2012)
28. R.D. Shannon, Revised effective ionic radii and systematic studies of interatomic distances in halides and chalcogenides. *J. Acta Crystallogr. A* **32**, 751–767 (1976)
29. L. Chowa, O. Lupana, G. Chaia, H. Khallafa, L.K. Ono, B.R. Cuenya, I.M. Tiginyanuf, V.V. Ursakif, V. Sontec, A. Schulte, Synthesis and characterization of Cu-doped ZnO one-dimensional structures for miniaturized sensor applications with faster response. *Sens. Actuators A* **189**, 399–408 (2013)
30. A. Hartmann, M.K. Puchert, R.N. Lamh, Influence of copper dopants on the resistivity of ZnO films. *Surf. Interface. Anal.* **24**, 671–674 (1996)
31. M.K. Puchert, A. Hartmann, R.N. Lamb, Highly resistive sputtered ZnO films implanted with copper. *J. Mater. Res.* **11**, 2463–2469 (1996)
32. J.B. Leea, H.J. Leea, S.H. Seob, J.S. Parka, Characterization of undoped and Cu-doped ZnO films for surface acoustic wave applications. *Thin Solid Films* **398**(399), 641–646 (2001)
33. X. Peng, J. Xu, H. Zang, B. Wang, Z. Wang, Structural and PL properties of Cu-doped ZnO films. *J. Luminesc.* **128**, 297–300 (2008)
34. I.N. Frantsevich, R.F. Voitovich, N.A. Lavrenko, *High-temperature oxidation of metals and alloys* (Gostekhizdat TLU, Kiev, 1963), p. 19
35. B.K. Dasa, T. Dasa, K. Parashara, S.K.S. Parashara, R. Kumarb, H.K. Choudhary, V.B. Khokhar, A.V. Anupamab, B. Sahoob, Investigation of structural, morphological and NTCR behaviour of Cu-doped ZnO nanoceramics synthesized by high energy ball milling. *Mater. Chem. Phys.* **221**, 419–429 (2019)
36. Y. Liu, J.H. Yang, Q.F. Guan, L.L. Yang, Y.J. Zhang, Y.X. Wang, B. Feng, J. Caoc, X.Y. Liub, Y.T. Yang, M.B. Wei, Effects of Cr-doping on the optical and magnetic properties in ZnO. *J. Alloys Compd.* **486**, 835–838 (2008)
37. S.Y. Seo, C.H. Kwak, S.H. Kim, S.H. Park, I.J. Lee, S.W. Han, Synthesis and characterization of ferromagnetic $Zn_{1-x}Co_xO$ film. *J. Cryst. Growth* **346**, 56–60 (2012)
38. P.P. Hankare, P.A. Chate, D.J. Sathe, P.A. Chavan, V.M. Bhuse, Effect of thermal annealing on properties of zinc selenide thin films deposited by chemical bath deposition. *Mater. Sci. Mater. Electron.* **20**, 374–379 (2009)
39. R. Anandhi, R. Mohan, K. Swaminathan, K. Ravichandran, Influence of aging time of the starting solution on the physical properties of fluorine doped zinc oxide films deposited by a simplified spray pyrolysis technique. *Superlattices Microstruct.* **51**, 680–689 (2012)
40. F. Ghahramanifard, A. Rouhollahi, O. Fazlolahzadeh, Electrodeposition of Cu-doped p-type ZnO nanorods; effect of Cu doping on structural, optical and photoelectrocatalytic property of ZnO nanostructure. *Superlattices Microstruct.* **114**, 1–14 (2008)
41. K. Hoggas, C. Nouveau, A. Djelloul, M. Bououdina, Structural, microstructural, and optical properties of $Zn_{1-x}Mg_xO$ thin films grown onto glass substrate by ultrasonic spray pyrolysis. *Appl. Phys. A* **120**, 745–755 (2015)
42. S.H. Wemple, M. DiDomenico, Behavior of the electronic dielectric constant in covalent and ionic materials. *Phys. Rev. B* **3**, 1338–2135 (1971)
43. E. Asikuzun, O. Ozturk, L. Arda, C. Terzioglu, Preparation, growth and characterization of nonvacuum Cu-doped ZnO thin films. *J. Mol. Struct.* **1165**, 1–7 (2018)
44. M. Caglara, F. Yakuphanoglu, Structural and optical properties of copper doped ZnO films derived by sol–gel. *Appl. Surf. Sci.* **258**, 3039–3044 (2012)
45. K.S. Ahn, T. Deutsch, Y. Yan, C.S. Jiang, C.L. Perkins, J. Turner, M. Al-Jassim, Synthesis of band-gap-reduced p-type ZnO films by Cu incorporation. *J. Appl. Phys.* **102**, 023517 (2007)
46. S. Roguai, A. Djelloul, Synthesis and evaluation of the structural, microstructural, optical and magnetic properties of $Zn_{1-x}Co_xO$ thin films grown onto glass substrate by ultrasonic spray pyrolysis. *Appl. Phys. A* **125**, 816 (2019)
47. Y. Liua, Q.Y. Hou, H.P. Xua, L.M. Lia, Y. Zhangb, First-principles study of the effect of heavy Ni doping on the electronic structure and absorption spectrum of wurtzite ZnO. *Phys. B* **407**, 2359–2364 (2012)

Publisher's Note Springer Nature remains neutral with regard to jurisdictional claims in published maps and institutional affiliations.